Article:
Zhu, X, Zhang, M, Yang, Y et al. (6 more authors) (2021) Understanding the aqueous phase of alkali-activated slag paste under bath-curing. Advances in Cement Research, 33 (2). pp. 59-73. ISSN 0951-7197

https://doi.org/10.1680/jadcr.18.00202

Accepted manuscript doi:
10.1680/jadcr.18.00202

Accepted manuscript doi:
10.1680/jadcr.18.00202

Submitted: 29 October 2018

Published online in 'accepted manuscript' format: 10 September 2019

Manuscript title: Understanding the aqueous phase of alkali-activated slag paste under bath-curing

Authors: Xiaohong Zhu[1,2], Mingtao Zhang[1], Yong Yang[1], Kai Yang[1,2], Fang Wu[1], Qing Li[1], Linwen Yu[1], Changhui Yang[1] and Muhammed Basheer[2]

Affiliations: [1]College of Materials Science and Engineering, Chongqing University, Chongqing, China and [2]School of Civil Engineering, University of Leeds, Leeds, UK

Corresponding author: Kai Yang, College of Materials Science and Engineering, Chongqing University, Chongqing, China.

E-mail: yang.kai@cqu.edu.cn, k.yang@leeds.ac.uk

Accepted manuscript doi:
10.1680/jadcr.18.00202

Abstract

The chemical compositions of aqueous phases in alkali-activated slag paste and Portland cement paste were determined up to 28 days with an aim at obtaining a better understanding of stability of hydration products in the two binder systems. The saturation levels with respect to hydration products of PC and AAS are approached through thermodynamic modeling. The main findings include: (1) the effective saturation indices for portlandite in AAS system is always below 0 and sulfate-bearing phases are not stable in AAS compared to those in PC; (2) the strätlingite and hydrotalcite phases should be stable in AAS due to the high [Mg] and [Si] concentrations in the pore solution; (3) both ionic strength and alkalinity of AAS pore solution are higher than those of PC, which are responsible for severer efflorescence in AAS paste and higher conductivity of AAS pore solution. According to thermodynamic estimation, T-based C–S–H is dominant in the AAS system after 7 days, while J- and T-based C–S–H gel were presented in PC system up to 28 days. It suggests that in PC and AAS, different solid phases are formed during the hydration, which change with time, and reactions and equilibria in both binders are completely different.

Keywords: Solution chemistry; chemical properties; Portlandite; alkali-activated cements

Accepted manuscript doi:
10.1680/jadcr.18.00202

1. Introduction

As by-product from iron production, ground granulated blast-furnace slag (GGBS) contains amorphous glassy phases which have a strong hydraulic potential (Richardson and Cabrera, 2000; Song and Jennings, 1999). By using proper activators, e.g. alkali metal silicates, hydroxides, carbonates or sulfates, GGBS can be activated to form the "binder" phase composited of "C–(N)–A–S–H", which can be named alkali-activated slag cement (AAS) (Ben Haha et al., 2011; Zhu et al., 2018). AAS generally shows a rapid strength development, high resistance to chemical attacks and possible high durability (Park et al., 2015; Yang et al., 2016). It, therefore, provides a latent economic and ecological superiority, which can be potentially used as "green binder" in the areas with severe carbon dioxide emission (Shi et al., 2011; Xu et al., 2015).

The main components of GGBS are SiO_2, CaO, Al_2O_3, and MgO, which mostly present in the glassy phase (Gong and White, 2016), while the crystal phases in GGBS are normally within 2%, which are mainly in Merwinite, Gehlenite, and Akermanite (Bougara et al., 2010). In some GGBSs, calcite and quartz are also found (Gong and White, 2016) that are commonly introduced by grinding. The reactivity of GGBS depends more on the glassy phases from its own composition point of view and the dissolution of the glassy phase and the introduction of sodium and silicate ions by Na-metasilicate (water glass, WG) can result in a complex composition of pore solution phases in WG-AAS. For the Portland cement (PC) system, the elements in the pore solution solely result from dissolution of clinker, gypsum or some cement admixtures. This difference leads to a result that the pore solution of WG-AAS has a higher Si concentration, but lower Ca concentration than that of PC (Gruskovnjak et al., 2006). In addition, the activation process of GGBS by strong or neutral alkali is believed to be a fast 'through solution' precipitation (Gruskovnjak et al., 2006), whilst the hydration of cement particle starts from its surface and through a 'dissolution-precipitation' process (Scrivener et al., 2015). As such, it is important to identify the changes in pore solution composition, which can provide essential information on the differences in instability of the solid phases in AAS and PC. The hydration products that presented in hydrated AAS and PC are different. As reviewed in a stoichiometric model by Chen (2006), the main hydration products that possibly presented in AAS include C–S–H, hydrotalcite, hydrogarnet, AFm phases (C_4AH_{13} and C_2ASH_8) and AFt, which depends on the type of activator. According to the XRD, TG, and SEM-EDX analysis of the WG-AAS solid phase (Zhu et al., 2017; Zhu et al., 2018), the presence of CSH(I) and hydrotalcite-like phase can be confirmed. Meanwhile, the absence of calcium hydroxide, AFt and AFm can also be proved. For PC, around 20% (by mass) calcium hydroxide generated during the hydration of silicate phases accompany with AFt, AFm (C_4AH_{13} and C_2ASH_8) phases generated by the following hydration of alumina clinker phases (Taylor, 1997). In addition, hydrotalcite-like phase is always found to intermix with C–S–H in slag-containing system, which depends on the Mg level (Richardson, 2018). The pore solution chemistry is of prime importance to understand the performance of cementitious materials. Firstly, the pH value (or alkalinity) of the pore solution affects the

Accepted manuscript doi:
10.1680/jadcr.18.00202

stability and redox potential of the passive film on the steel surface, which is believed to directly affect corrosion (Criado et al., 2017). Another related problem is the efflorescence of AAS due to the high alkali brought by the activators that was not fully combined with the hydration products (Provis et al., 2015). Further, the ions concentrations in pore solution of the cementitious materials are also considered to have an influence on the diffusion of chloride, sulfate ions due to the 'ionic effect' (Ma et al., 2015). The composition of the pore solution defines the water activity of the internal solution in mesopores, thus deciding the Kelvin radius of concrete (Ye and Radlinska, 2017), which could affect the shrinkage behaviors of AAS concrete (Zhu et al., 2018). Last but not least, the adsorption of carbon dioxide is also affected by the composition of ions in the pore solution (Yu, 2012). Another use of the pore solution conductivity is to assess the pore connectivity through electric responses (Zhu et al., 2018). Although this method only requires the conductivity of pore solution, the understanding of the solution compositions provides the reasons behind the conductivity, as it is closely related to the ionic strength in the aqueous (Kempl and Çopuroğlu, 2016). Examination of important factors of the aqueous phases of AAS offers a key approach to assess on its performance. Therefore, two series (PC and AAS) of pastes with water to binder (w/b) ratios of 0.35 and 0.50 were prepared, the pore solutions were of which were collected through high-pressure device. A study of the element concentration, ionic strength, pH and effective saturation indices (ESI) for portlandite in AAS is reported and solubility relationships in both AAS and PC binder systems are modeled using the concentrations of ions in pore solution.

2. Theoretical considerations and modeling approach

Thermodynamic modeling, which describes connections between aqueous and solid phases, is considered as one of the most powerful tools to assess the stability (solubility) of solid phases in the cementitious system (Lothenbach, 2010; Damidot et al., 2011). The law of mass action (LAW) and minimising the Gibbs free energy (GEM) of the system are two techniques to achieve thermodynamic estimation. The first principle is coded in the software such as PHREEQC, MINEQL, EQ3/6 or CHESS (Lothenbach, 2010), while the second one is given in GEMS (Kulik et al., 2012). It is found that the two approaches, LAM and GEM, give comparable results (Lothenbach, 2010; Kulik et al., 2012; Tres Thoenen et al., 2014). Thermodynamic modeling solid phases through pore solution compositions at the saturation level requires an assumption of local equilibrium condition, which means comparing to dissolution and precipitation processes, the ionic transport is negligible. The first step to calculate relevant equilibria is to determine the thermodynamic activity of each ion in the complex solution. In the analytical chemistry, the ion activity of individual species (a_i) is defined as its molality (m_i) multiplying by the activity coefficient (γ_i):

$$\boldsymbol{a_i = \frac{m_i}{m_0}\gamma_i} \quad \text{Equation 1}$$

The activity of ion is affected by formation of complexes in the system, which will reduce its value. Taking the [Ca^{2+}] as an example, the formation of $CaOH^+$, $CaSO_4^0$ can reduce its

Accepted manuscript doi:
10.1680/jadcr.18.00202

activity. Therefore, it is important to carry out a complete testing of the ions presented in the pore solution which will improve the accuracy in thermodynamic calculations. The m_0 in Equation 1 stands for the standard concentration (1 mol/kg), which can be ignored during the calculation process.

Davies (Equation 2) and Extended Deby-Hückel (Equation 3) equations are the most common models used in cement pore solution to estimate activity coefficient:

$$\boldsymbol{log\,\gamma_i = -A_\gamma z_i^2\left(\frac{\sqrt{I_m}}{1+\sqrt{I_m}} - 0.3I_m\right)} \quad \text{Equation 2}$$

$$\boldsymbol{log\,\gamma_i = \frac{-A_\gamma z_i^2\sqrt{I_m}}{1+ \text{å}B_\gamma\sqrt{I_m}} + b_\gamma I_m} \quad \text{Equation 3}$$

$$\boldsymbol{I_m = \frac{1}{2}\sum m_i z_i^2} \quad \text{Equation 4}$$

where, I_m is the effective molal ionic strength, which was defined in Equation 4, Z_i is the charge of the ion i, A_γ and B_γ are two constants related to the temperature and pressure, which have values of 0.51 and 0.33 at 25 °C and standard atmospheric pressure (1 atm), $\dot{a}$ and b_γ are two parameters individually for different ions by measuring and fitting with the activity of pure salt solutions. Table 1 lists values of $\dot{a}$ and b_γ of some ions related to cement solution (https://www.usgs.gov/software/phreeqc-version-3).

Note that when not all fitting parameters are not known, Davies equation is normally implemented. It needs to be pointed out that Equation 1, 2, 3 and 4 are only suitable for the solutions with ionic strength in the range of 0.1 to 0.5 molal. When ionic strength is higher than 1.0, specific ion interaction term (SIT) or the Pitzer model should be considered (Kulik et al., 2012; Lothenbach et al., 2008). According to the results reported by Thomas and co-workers (Thomas et al., 2003; Rothestein et al., 2002), the ionic strength of the pore solution in cement samples is normally within 0.5.

Table 2 gives the ions activity products (IAP) equations and the solubility products (K_{sp}) values (25 °C) at the equilibrium condition used in this study. These values are collected from the previous works (Lothenbach et al., 2010; Thomas et al., 2003; Rothestein et al., 2002; Lothenbach et al., 2008) and coded into PHREEQC database. The temperature dependence of the K_{sp} is assessed using van Hoff equation:

$$\boldsymbol{\ln\left(K_{sp}\right) = \ln\left(K_{sp25c}\right) + \frac{\Delta H_r}{R}\left(\frac{1}{298} - \frac{1}{T}\right)} \quad \text{Equation 5}$$

where ΔH_r stands for the enthalpy of reaction (kJ/mol, defined in Equation 6 and given in Table 2), R is the gas constant (8.314 J·mol^{-1}·K^{-1}) and T is the Kelvin temperature (K).

$$\boldsymbol{\Delta H_r = \sum \Delta H_{f,products} - \sum \Delta H_{f,reactants}} \quad \text{Equation 6}$$

where ΔH_f is the standard formation enthalpy (kJ/mol).

With the definitions above, the saturation indices (SI) can be expressed as follows:

$$\boldsymbol{SI = \log\frac{IAP}{K_{sp}}} \quad \text{Equation 7}$$

when IAP equals K_{sp}, the SI equals to 0 and the equilibrium condition is considered to be reached. An SI with the value higher than 0 indicates that the solution is supersaturated with

Accepted manuscript doi:
10.1680/jadcr.18.00202

the respective solid phase and the related solid phase has the potential to precipitate. When an SI is less than 0, the solution is undersaturated with the relevant solid phases and the solid prefers to dissolve. Further, the effective SI (ESI) is defined as dividing the SI by the number of ions participating in the reactions (given in Table 2) to form the solids. For example, these numbers in gypsum, portlandite and ettringite are 2, 3, and 15 respectively (Lothenbach et al., 2008). The PHREEQC interaction V3.4.0 was used in this study to calculate SI and other thermodynamic properties of pore solutions. A database specially coded for the solid phases in cement was used and some related parameters are given in Table 2. Since C–S–H is the main hydration products in both system, two types of C–S–H are chosen for comparison through thermodynamic calculation. The main difference in hydration product between AAS and PC hydrates is calcium hydroxide, which should be discussed in details. Three typical AFm phases (manosulphoaluminate, hydrotalcite and Strätlingite) and AFt were also discussed due to their uncertainty of presence in both systems.

3. Experimental details

3.1 Raw materials

Raw granulated blast-furnace slag (GGBS) was provided by Chongqing Iron & Steel Company. The obtained GGBS has a Blaine fineness of 430 m^2/kg and a density of 2.80 g/cm^3. Portland cement (PC) confirms to the stipulations in GB 175 (2007) that has a Blaine fineness of 335 m^2/kg and a density of 3.15 g/cm^3. The chemical compositions of GGBS and PC are given in Table 3. It should be noted that the sulfate content of GGBS shown in the Table 3 is only 0.23%. This is because the chemical compositions reported here were determined using chemical methods specified in Chinese standard GB/T 176 (2008) and most sulfur in GGBS remains sulfide due to the reducing atmosphere in the iron production process (Arai et al., 2017; Ray, 2009). Comparing to GGBS, PC has a sulfate content of 2.58% is mainly due to the presence of gypsum for controlling setting behavior (Zhu et al., 2018).

The alkali content (Na_2O equivalent) used in this study was selected as constant 5% by mass of GGBS. Liquid sodium silicate (water glass, WG) with a modulus (defined as the mole ratio of SiO_2 to Na_2O) of 1.20 was selected as the activator for AAS. Dry pellet NaOH was used for adjusting the liquid sodium silicate from the initial modulus of 2.48 to 1.20. To avoid the exotherm introduced by the dissolution of alkali, the dry pellet NaOH was firstly dissolved in deionized water and cooled down in room temperature before mixing with sodium silicate solution. The obtained solution was further cooled in a room at a constant temperature of 20 ± 2°C for 2 h prior to mixing paste.

3.2 Sample preparation and pore solution extraction

The mix proportions of AAS and PC pastes are summarised in Table 4. Two water/binder (w/b) ratios are used. The calculation of w/b ratio for AAS includes both the water from the activator and external water. The pastes were cast into a specific cylinder mold (as shown in Figure 1) for the purpose of extraction of pore solution in the device. The pastes with 0.35 w/c ratio are vibrated on a vibration table until no bubbles appeared on the surface. The

pastes with 0.50 w/c ratio are vibrated manually to avoid over-vibration, which may result bleeding on the surface. Even so, a slight bleeding also happens for high w/c ratio pastes. All specimens were de-molded after 24 h curing in a standard room with a constant temperature of 20 ± 1°C and a relative humidity (RH) ≥ 95%. After de-moulding, the specimens were further transferred into a water tank for further curing until testing ages. The reason for curing in the water is that this condition is more suitable for the assessment of pore connectivity in another study (Zhu et al., 2018).

Extraction of pore solution from paste specimens was performed in a high-pressure device (SBT, CO., LTD.) in conjunction with a compression machine (1000 kN). This method was firstly described by Longuet et. al (2015). Before pore solution extraction, the cylinder pastes were removed from the water tank to a standard room (20 ± 1°C, RH ≥ 95%) for 24 h to achieve saturated surface dry state. The paste cylinder was put into the chamber of the high-pressure device and extracted under a constant pressure of 407.6 MPa (800kN over 1962.5 mm^2) for 45 min. The pore solution was collected in a vacuum collector chamber to avoid carbonation and stored in a low-temperature box (5°C) to avoid the precipitation of calcium-containing compounds.

3.3 Pore solution analysis

The obtained pore solutions (3d, 7d, 14d, and 28d) were firstly filtered through a nylon filter (0.45 μm) to remove remaining solids that may block the plastic tube in inductively coupled plasma optical emission spectroscopy (ICP-OES). The pH value (pHS-3C, INESA) of the pore solution was tested immediately after filtering. The pH electrode was calibrated using a standard solution with pH values of 6.86 and 9.18. The pH value is determined through Nernst function by using electrode method as expressed in Equation 8.

$$E = \left(\frac{2.303\mathrm{RT}}{F}\right)(\mathrm{pHi} - \mathrm{pHs}) + E\mathrm{as} \quad \text{Equation 8}$$

where, E is potential difference (V); R is the gas constant; T is the temperature (K); F is Faraday's constant; pHi is the pH value of buffered solution in pH probe (=7); pHs is the tested pH value; E_{as} is the asymmetric potential (V).

The total concentrations of elements (Na, K, S, Al, Ca, Mg, Si) were analysed by ICP-OES (ThermoFisher Scientific, Germany). Every sample was tested thrice by ICP-OES and the average results were recorded as the final ions concentrations. The concentrations of K^+, Na^+, Mg^{2+} and Ca^{2+} were tested using mix-standard solutions while the other elements were measured using sole-standard samples. The standard solutions for ICP-OES were purchased from the Chinese standard substance website (http://www.crmrm.com/). It should be noticed that optically pure solution should be selected for the ICP-OES. The positive ions with similar range of concentration can be calibrated together as stated above. Normally, five points were used for the calibration of one ion, which will form a linear line. The pore solution should be diluted to a certain concentration level to assure the testing point falls on the calibration curves. If the testing concentration is beyond or below the calibration curve range, another dilution factor was chosen for testing again to make sure that the value is distributed along the linear calibration line. Since the sulfur presented in slag samples are

mostly in sulphate (SO_4^{2-}), its concentration in AAS pastes pore solutions was determined by ion chromatography (IC). The differences between total sulphur and sulphate was calculated as the sulphide (S^{2-}) concentration.

4. Results and discussions

4.1 Element concentrations

The major elements presented in the pore solutions of AAS and PC paste are shown in Figure 2. The curves in individual figures (except Mg) in Figure 2 represent statistic calculated mean values and 95% confidence interval, which were the statistical results of pores solution compositions of CEM I (according to EN 197-1) reviewed by Vollpracht et al. (2015) and were used as a guidance for the experiments results in this investigation. Unsurprisingly, the AAS or PC paste with a higher w/b ratio generally gives a lower OH^- concentration, which mainly due to the dilution of more added water. Meanwhile, the sodium (Na) concentration in AAS pore solution is almost one order magnitude higher than that in PC pore solution. The reason is that the slag was activated by 5% Na_2O_{eq} alkali (as shown in Table 4) which cannot be consumed sufficiently, while Na^+ in PC mainly came from Na_2O in clinker (0.21%). The similar results were also found in the pore solution of a Na-metasilicate pentahydrate activated slag paste, which gave approximately 1300 to 1500 mmol/L Na^+ concentration at the age around 180 days (Gruskovnjak et al., 2006). Comparing to the existing data, a relatively low Na^+ concentration in this study was obtained, which may be due to the dilution effect caused by the curing regime applied. The concentration of Na^+ in PC pore solution mainly came from the hydration of clinker that depends on the source of raw clinker ores (Taylor, 1997). For example, the orthorhombic and monoclinic C_3A can bind certain Na for charge balancing, which will be released when the hydration°Ccurs (Myers et al., 2017). Thus, the Na^+ concentration in PC pore solution often increases steadily as the hydration degree or hydration time increases. This trend is clearly shown in the statistical results in Figure 2. However, the experiments result of Na^+ concentration in PC pore solution did not increase, since the water immersion curing regime was applied and certain ions may diffuse into the curing water. In addition to this, the Na_2O content (Table 3) of the PC used in this experiment is only 0.21%, which reaches the lower limit of the statistical analysis. Therefore, a relatively close experimental Na^+ concentration to the 95% lower confidence interval of the statistical calculation was obtained. Potassium (K) is another alkali-metal in both slag glassy phase and clinker phase. Due to low combination ratio by hydration products (Sun et al., 2018), most K are presented in the liquid phase. The K concentration in AAS pore solution is much lower than that in PC pore solution. The main reason is the initial K_2O content in PC and slag are 0.70% and 0.46%, as given in Table 3. Even though, the total alkaline metal ions in AAS pore solutions are still greatly higher than those in the PC pore solution.

In AAS paste, abundant hydroxide ions (OH^-) were introduced by the activator and consumed, when the chemical bonds in slag were broken due to its chemical polarity. In this process, partial OH^- ions still remain in the solution for the charge balancing with cation ions. The situation for PC paste is different, because alkali cations presented in either sulfates or

the major clinker phase released with the ongoing hydration and the balancing anion entered a hydration product with low solubility later (Taylor, 1997). Thus, the equivalent amount of OH^- was released and existed in the liquid phase of paste to achieve its alkalinity. The high OH^- concentration in pore solution can maintain the alkaline environment for a concrete structure, which is vital for its durabilities, e.g. limiting the speed of reinforce corrosion (Yu et al., 2015). The results showed in Figure 2(c) indicate that the OH^- concentration in pore solution of 5%-Na_2O activated slag sample is higher than that in PC pore solution in regardless of curing age.

Another abound element that presented in AAS and PC pore solutions is sulphur. However, the ratio of sulphide to sulphate in these two solutions are totally different because of the sulphur sources. It is well known that the sulphur species can exist as sulphide or sulphate in GGBS (Roy, 2009; Sangha et al., 1992). Roy (2009) pointed out that a small amount of oldhamite (CaS) was always presented in the original slag and the oldhamite was found both as independent crystals or merged with melilite, which is one main source of sulphur in GGBS. Therefore, the sulfate to sulfide ratio depends on the cooling regime of GGBS, as the slow-cooling can result in the oxidation of CaS (Arai et al., 2017; Ray 2009). Due to the extremely high alkaline condition, the sulphur prefers to be sulphide (S^{2-}) in AAS pore solution that could assist reducing some hazardous ions, e.g. hexavalent chromium (Zhang et al., 2008; Zhang et al., 2017). However, as shown in Figure 2(d), the sulphur element concentration in PC pore solution stays close to the mean value of the statistic calculation and generally shows a decreasing trend as a function of time. Some sulphur in PC clinker was brought by the use of coal-fired manufacturing technique (Arai et al., 2017) and normally combined with metal cation, such as arcanite (K_2SO_4), thenardite (Na_2SO_4), aphthitalite ($(K,Na)_3Na(SO_4)_2$) or anhydrite ($CaSO_4$) (Sun et al., 2018). More importantly, gypsum (3% to 5% by mass of clinker) was added to clinker in order to control the setting behaviour through reactions with aluminate phases (C_3A) (Myers et al., 2017). Thus, the sulphur species that presented in PC solution was mainly sulphate ions. The experimental results shown in Figure 2(d) agree on the analysis above. It is clear that the sulphur element concentration in AAS pore solutions was much higher than that in PC pore solutions and most of the sulphur in AAS pore solutions were not sulphate. The sulphate concentration in PC pore solutions was lower than 10 mmol/L, while the total sulphur in AAS pore solution was several tens millimolar. These results are consistent with the sulphur speciation results obtained from S K-edge X-ray absorption near edge structure spectroscopy (XANES), which gave that the sulphur in GGBS was composed by 57% sulphide, 37% S(0), 3.81% sulphate and 2.33% sulphonate (Arai et al., 2017). It is noted that the sulphur element concentration in AAS pore solution was lower than that in the study performed by Gruskovnjak et al. (2006) and the main reason is believed to be due to difference in the sulphur content in the original GGBS.

The rest four elements (Si, Al, Ca, and Mg) are trace in both AAS and PC liquid phases. The hydration products containing these four elements show very low solubility (Table 2). Even though, the differences between these element concentrations in AAS and PC pore solutions are significant. Concentrations of [Si], [Al], and [Mg] in AAS pore solution are much higher

Accepted manuscript doi:
10.1680/jadcr.18.00202

than those in PC pore solution. The [Si] in AAS liquid phase mainly introduced by the water glass, whereas that presented in PC pore solution came from the dissolution of silicate phases. In regard of [Al] and [Mg], GGBS contains much higher chemicals (Al_2O_3 and MgO) in raw material than those in PC, which results in a higher concentration in solution phase. In contrast, the [Ca] in AAS pore solution is extremely low, which was under 1 millimolar. In addition, the [Mg] in both AAS and PC pore solutions is trace since the Mg-bearing hydration products have an extremely low solubility.

4.2 Ionic strength and alkalinity of pore solution

The ionic strength of a pore solution is regarded as a major variable in examining the "slat effect" in many science fields (Vicente 2004). It is proposed in 1921 by G. N. Lewis and M. Randall and defined by Equation 4, which is the basis of the high concentration solution chemistry and becomes one key factor together with temperature, pressure and pH (Vicente 2004). In AAS and PC pore solutions, the ionic strength can be used to calculate the activity coefficient and the solubility behaviors of hydration products. Due to the high concentrations of K^+, Na^+ and OH^- in pore solutions of AAS and PC pastes, the electrical conductivity can be estimated from these ions (Snydera et al., 2003), since the electrical conductivity of a solution is directly linked to its ionic strength (Rajabipour and Weiss, 2006). The calculated ionic strength development of both AAS and PC pore solutions as a function of sample age are shown in Figure 3(a). The results clearly show that the ionic strength of all pore solutions decreased as increasing curing time, which is mainly due to the decreasing alkali metal ions caused by leaching in the water curing regime. It is also found that the changes in ionic strength of AAS pore solutions are more pronounced than that of PC solutions. The reason is that the highly movable Na^+ concentration drops dramatically as curing time went on (Figure 2(a)) and AAS does not have $Ca(OH)_2$ that serves as a buffer of ionic concentration (Gruskovnjak et al., 2006). According to the study of Rothstein et al. (2002), the ionic strengths of PC and white Portland cement (wPC) were around 0.30-0.50 and 0.10-0.20 throughout the hydration. The results in this study are 0.25-0.35 for PC pore solution, which is close to the reported data. It needs to be pointed out that the ionic strength of the pore solution in 0.35 w/b ratio AAS almost reached 0.90 initially and then dropped around 0.50 after 14 days. For the higher w/b ratio, AAS pore solution has an ionic strength initially from 0.55 and equilibriums at 0.30-0.35 thereafter. Similar to the changes of ions concentrations in solutions, the higher w/b ratio also gave a lower ionic strength of pore solution due to the dilution effect. This results also confirm the electrical conductivity results of both AAS and PC pore solutions as described in the authors' previous work (Zhu et al., 2018).

The total alkalinity of pore solutions was calculated based on the standard carbonate compounds, which refers to the proton binding capacity of the solutions. Normally, in a solution system at any pH, there are proton acceptors ($[HCO_3^-]$, $[CO_3^{2-}]$,$[OH^-]$) and proton donors ($[H^+]$). This excess of proton acceptors over donors with respect to the chosen zero level of protons is defined as the total alkalinity (as shown in Equation 9). These concepts are

Accepted manuscript doi:
10.1680/jadcr.18.00202

originally coded into PHREEQC and were just used as an indicator of alkalinity in this system.

$$\mathbf{TA = proton\ acceptors - proton\ donors} = [\boldsymbol{HCO_3^-}] + \mathbf{2}[\boldsymbol{CO_3^{2-}}] + [\boldsymbol{OH^-}] - [\boldsymbol{H^+}]$$

Equation 9

The development trend of total alkalinity in both AAS and PC pore solutions was similar to that of ionic strength, because it is also mainly determined by the hydroxide concentrations in solutions. The results in Figure 3(b) shows that the alkalinity of the AAS pore solution is much higher than that of PC pore solution, which is one main reason that why AAS has a severer efflorescence than PC (Provis et al., 2015). Another trend in Figure 3(b) is the lower calcium ions in AAS pore solutions that could increase efflorescence, as the presence of calcium ions was important for reducing the alkali mobility (Lloyd et al., 2010; Lee et al., 2018; Oh and Choi, 2018).

4.3 Saturation levels of minor and trace hydration products

The hydrated AAS and PC contains complex hydrates. In this section, the saturation levels of minor and trace hydration products, including calcium hydroxide (CH), ettringite (AFt), monosulphoaluminate (AFm), strätlingite (C_2ASH_8), and hydrotalcite-like phase (MAH_{10}), were calculated according to their thermodynamic properties (Table 2). The effective saturation index (ESI) development of each phase was plotted in Figure 4 as a function of time. In order to compare with results from other studies (Rothestein et al., 2002; Lothenbach et al., 2008), ions concentrations in pore solution of PC, wPC, and AAS were also analysed. These results were also plotted in Figure 4 and were used as the guidance for the ESI calculated in this investigation. As few Mg concentration data were found in the literature, the ESI of Mg-bearing phase (hydrotalcite) was calculated using the data obtained in this study.

Calcium hydroxide (CH) is one of the main hydration products of C_2S and C_3S, which takes up more than 20% (by mass) in the PC system (Taylor, 1997; Richardson et al., 2016). However, very few CH can be found in the AAS system, because of the lack of calcium (Myers et al., 2015). The ESI development of CH was shown in Figure 4. As expected, all ESIs of PC pore solutions were over zero, which means that the pore solution is always oversaturated with CH in regardless of hydration time. A slight decreasing trend was found for the ESI of CH in PC pore solution as a function of time and it was mainly because of decreasing the concentration of Ca. These results agree with the ESIs calculated using GEMS database (De Weerdt et al., 2011). On contrary, the ESI for portlandite in AAS pore solutions were below zero, which means that at most times, AAS pore solution is undersaturated with CH. In other words, the CH is not possible to participate in a such environment and it explains why no solid CH was found in the hydration products of AAS system. The stability of CH is defined by the activity of $[OH^-]$ and $[Ca^{2+}]$ in the solution. The results in Figure 2 indicated that the $[OH^-]$ concentration in AAS pore solutions is always higher than that of PC pore solution, while the $[Ca^{2+}]$ is much lower. The residual $[OH^-]$ in AAS aqueous phase was balanced by $[Na^+]$ and $[K^+]$, not $[Ca^{2+}]$ in the solution. Therefore, the portlandite can exist in

Accepted manuscript doi:
10.1680/jadcr.18.00202

the AAS system, only when extra CaO or gypsum was added according to the thermodynamic calculation performed by Ye and Radlińska (2017).

With regard to the sulphate-bearing phases, AFt and AFm are most common as the hydration products formed from the reactions between C_3A and gypsum in the PC system. For these complex hydrates, [Ca], [Al], [SO_4^{2-}], and [OH^-] are essential for their formation and stability. It is clear from the results in Figure 4 that the pore solution of PC pastes kept oversaturated to both AFt and AFm all the time and no decreasing trend was observed, which means these phases are relatively stable in the PC system. However, the presence of AFm and AFt in AAS system is controversy, as most ESIs for sulphate-bearing phases obtained from this study were lower than zero, meaning an under-saturation solution environment. The main reason is that most of the sulphur presented in this AAS was sulphide instead of sulphate as discussed in Section 4.1. Interestingly, the calculated ESIs of both AFm and AFt based on data collected from Gruskovnjak et al. (2006) were always higher than zero, which means AFm and AFt may be found in the AAS system. The main difference in element concentration of the aforementioned and present studies are sulphate concentrations, which depends on the source of GGBS and the cooling regime. It should also be noticed that AFt was always found in AAS system when sulphate was sufficient, especially when the activator contains sulphate salts (Ye and Radlińska, 2017; Bakhareva et al., 2002) or AAS was explored in sulphate environments (Bakhareva et al., 2002). These results also prove that sulphate-bearing phases, AFt or AFm, are possible to present in AAS.

Strätlingite (C_2ASH_8) is a kind of silicon-bearing trace hydration product in some pozzolanic materials added PC system (Lothenbach et al., 2011). This hydrate depends on the concentrations of [Ca], [Al], [Si] and [OH^-] in pore solution. Normally, due to the lack of [Si] in the pure PC system, strätlingite often forms at the latter age or when additional siliceous phases were added (Lothenbach et al., 2011; Midgley and Rao, 1978). It needs to be pointed out that the presence of strätlingite in both AAS and PC is difficult to be detected by direct techniques, such as powder X-ray diffraction or scanning electron microscopy (Jia and Richardson, 2017) and indirect methods (analysis of pore solution) is a common approach to assess its presentence. The ESI results in Figure 4 show that strätlingite can present in pore solutions of both AAS and PC. In addition, the ESI for strätlingite in the AAS is higher than that of PC due to a higher [Si] and [Al] concentrations. Analysis of data collected from Rothstein et al. (2002) indicates an undersaturated condition initially and a trend for strätlingite participation was found after 20 days accompanied with the release of [Si].

The MgO content in GGBS can vary from 1% to more than 9% by mass, which is essential for the formation of Mg-bearing phases in AAS system (Bernal et al., 2014). The hydrotalcite-like phase is proved as an Mg-bearing phase as a hydration product in slag-containing samples (Zhu et al., 2017; Chen et al., 2004) and the calculated results show that the ESIs for hydrotalcite phase are always above 1, which means it is easy to form if all the essential ions are available in the solution due to the extremely low solubility. Moreover, the ESI for hydrotalcite in AAS is much higher than that of PC due to the higher [Mg] concentration in the solution phase as stated in Section 4.1.

Accepted manuscript doi:
10.1680/jadcr.18.00202

4.4 Solubility behavior of C–S–H

Calcium silicate hydrates (C–S–H) gel in hydrated cement possess a remarkable level of structural complexity and its solubility behavior intricately relates to the corresponding structure (Chen et al., 2004). More specifically, the [Ca] and [Si] in the contacting aqueous phase (pore solution) should be tied thermodynamically to the underlying solid structure (Chen et al., 2004). Since there is no widely accepted equilibrium solubility of C–S–H, the ESI is not a fixed value (Rothestein et al., 2002). There are two types of C–S–H that were widely used in previous studies, i.e., tobermorite-based (T-based) and jennite-based (J-based) C–S–H (Lothenbach, 2010; Lothenbach et al., 2008; Richardson, 2004; Kulik, 2011). The ions activity products (IPA) equations and the thermodynamic properties are listed in Table 2, which were used for the calculation of ESI in this investigation. Although this approach did not take the complex compound $CaOH^+$ into consideration compared with other IPA equations (Rothestein, 2002), these equations were used in most thermodynamic calculations in cement science (Lothenbach, 2010; Damidot et al., 2011; Lothenbach and Winnefeld, 2006). The obtained ESI results combined with the data recalculated from the literature are plotted in Figure 5 for both T- and J-based C–S–H.

It is well known that T-based C–S–H possess a lower Ca/Si ratio, while J-based C–S–H has a higher Ca/Si ratio. Meanwhile, the J-based C–S–H has a lower equilibrium solubility product than that of T-based C–S–H, meaning that it is easy to form when Ca^{2+} is sufficient. Therefore, the difference in the IPA equations of these two C–S–Hs is the contents of Ca^{2+} ions. As shown in Figure 5, the ESI for the J-based C–S–H gel in the PC system is much higher than that of the AAS system, which mainly resulted from the low Ca^{2+} concentration in the AAS pore solution. However, the ESI of J-based C–S–H in AAS was much higher than 0 at the early age due to the rapid Ca released from slag, then gradually equilibrated at 0. For the PC system, the ESI for J-based C–S–H always stays above 0 and equilibrated at around 0.20. With respect to the T-based C–S–H gel, the ESI for both PC and AAS pore solution is higher than 0, which means that the T-based C–S–H tends to precipitate in both systems. It is noticed that some results collected from the previous data indicate that ESI for T-based C–S–H in the PC system is lower than 0. The main reason is attributed to the low Si concentration in the pore solution, which can cause the instability of T-based C–S–H.

The results shown in Figure 5 also indicate that both J- and T-based C–S–H gel were presented in PC system up to 28 days, whilst T-based C–S–H is dominant in the AAS system after 7 days. The studies of the structure of C–S–H gels in slag-cement (Richardson and Cabrera, 2000) or KOH-activated slag (Richardson and Li, 2018) showed a possible linking to T-based structure C–S–H, which is consist to the thermodynamic stability results in this investigation. Moreover, the evidences from the insights of C–S–H structures (Chen et al., 2004) led to the hypothesis that C–S–H gel in PC system initially has a mixture of T- and J-based structure, whilst dominated by the J-based structure in the middle age and then solely presented as the jennite-like structure at the very late age. These analyses also agreed with the instability of T-based C–S–H in this simulation, while both T- and J-based are still present up to 28 d.

Accepted manuscript doi:
10.1680/jadcr.18.00202

Figure 6 plots OH^- against Ca^{2+} concentrations in both AAS and PC pore solutions and the dashed line was calculated from the solubility products of CH at 20°C, which was used as a guidance of the relationships between Ca^{2+} and OH^-. Since the current data were obtained from a multicomponent system, which contains both CH and other Ca-bearing hydration products, and hence the Ca^{2+} ions are much higher than the equilibrium curve of CH at certain OH^- concentration (Vollpracht et al., 2015). Generally, the calcium concentration decreased as the OH^- concentration increasing due to the common ions effect. The scatter points in Figure 6 indicate that the calcium and hydroxyl ions in PC pore solution are much oversaturated with respect to CH, whilst those in AAS are just around the equilibrium curve of CH. This relationship also supported the ESI results that CH is not stable in AAS pore solution environment.

As shown in Figure 7, Jennings plotted an array of C–S–H solubility data from the existing literature and two solubility curves (two dash lines) of C–S–H were given, which suggested the thermodynamic equilibrium condition of the C–S–H. Although two curves were obtained, the reasons for their formation are still controversial. The curve A with the lower Si concentration in Figure 7 was normally considered as the metastable solubility curve for C–S–H (I) with the lower Ca/Si ratio (i.e., T-based C–S–H gel) (Jennings, 1986). The formation of curve B with a higher Si concentration was not directly related to C–S–H (II), but argued to be the presence of a superficially hydroxylated surface on C_3S (Chen et al., 2004). The ion concentration results from this investigation and the data collected from the literature were also plotted in Figure 7. It is clear that all the points are divided into three clusters, which are the ion concentrations of AAS, PC, and wPC pore solutions. Interestingly, all AAS and PC points distributed along Curve A and certain differences in Ca and Si concentration can be found. For the wPC, the pore solution points stay between Curve A and Curve B. Since the Curve A can be related to C–S–H (I), these results strongly suggest that T-based C–S–H is dominated in AAS. The solubility of C–S–H formed in PC also resides on Curve A, which may indicate that Curve A cannot be solely attributed to C–S–H (I) but for also for the C–S–H mixtures. The migration of the solubility of C–S–H in wPC mainly attributed to the higher C_3S content (normally around 70%) in raw materials (Richardson et al., 2016).

5. Conclusions

The pore solution chemistry of AAS and PC pastes are analysed through ICP-OES and IC. The element concentrations are obtained and the thermodynamically stability of hydration products are modeled and discussed. The main conclusions can be drawn as below:

1. The 5% Na_2O-WG-AAS pore solution has a fairly high [Na], [S], [Si], [Al], and [Mg] element concentrations but low [K] and [Ca] element concentrations in comparison with PC up to 28 days. The pH values of the AAS pore solution are higher than that of PC at the same condition.
2. AAS pore solutions give higher ionic strength and total alkalinity than those of PC, while a higher w/b ratio can dilute the ionic strength and alkalinity of pore solution in both AAS and PC systems.

3. The ESI of portlandite in AAS system is always below 0. Thus, portlandite is not possible to form in this solution environment. Meanwhile, it is also found that sulfate-bearing phases (AFt and AFm) are not stable in the AAS. However, strätlingite and hydrotalcite can be present, since the [Si] and [Mg] concentrations of AAS are much higher than those in PC pore solution.
4. Both J- and T-based C–S–H gel were presented in PC system up to 28 days, whilst T-based C–S–H is dominant in the AAS system after 7 days.

Acknowledgements

The authors acknowledge the following institutions for providing facilities and the financial support: National Natural Science Foundation of China (NO. 51878102 and 51778089), Open funds from Shenzhen University, State Key Laboratory of High Performance Civil Engineering Materials, Chongqing Jiaotong University, Chongqing Foundation Research Program. In addition, supports provided from University of Leeds during analysis of data and preparation of this paper are also highly appreciated.

Notation list

a_i the ion activity of individual specie (i)

m_i the molality of the ion i (mol/kg)

m_0 the standard concentration, 1 mol/kg

γ_i the activity coefficient of the ion i

A_γ the constant related to the temperature in Equation 2

B_γ the constant related to the pressure in Equation 3

I_m the effective molal ionic strength (mol/kg)

Z_i the charge of the ion i

$\dot{a}$ the parameter individually for different ions by measuring and fitting with the activity of pure salt solutions in Equation 3

b_γ the parameter individually for different ions by measuring and fitting with the activity of pure salt solutions in Equation 3

K_sp the solubility products

K_sp25c the solubility products at 25°C

ΔH_r the enthalpy of reaction (kJ/mol)

R the gas constant, 8.314 J·mol^{-1}·K^{-1}

T the Kelvin temperature, K

Accepted manuscript doi:
10.1680/jadcr.18.00202

ΔH_f the standard formation enthalpy (kJ/mol)

$\Delta H_{f,products}$ the standard formation enthalpy of reaction products (kJ/mol)

$\Delta H_{f,reactants}$ the standard formation enthalpy of reaction reactants (kJ/mol)

IAP the ion activity products

SI the saturation indices

ESI the effective saturation indices

E the potential difference (V)

F Faraday's constant (C/mol)

pHi the pH value of buffered solution in pH probe (=7)

pHs the tested pH value

E_{as} the asymmetric potential (V)

References

Arai, Y., B.A. Powell, and D.I. Kaplan, Sulfur speciation in untreated and alkali treated ground-granulated blast furnace slag. Sci Total Environ, 2017. 589: p. 117-121.

Bakhareva, T., Sanjayana, J.G., and Cheng, Y.-B. Sulfate attack on alkali-activated slag concrete. Cement and Concrete Research, 2002. 32: p. 211-216.

Ben Haha, M., et al., Influence of activator type on hydration kinetics, hydrate assemblage and microstructural development of alkali activated blast-furnace slags. Cement and Concrete Research, 2011. 41(3): p. 301-310.

Bernal, S.A., et al., MgO content of slag controls phase evolution and structural changes induced by accelerated carbonation in alkali-activated binders. Cement and Concrete Research, 2014. 57: p. 33-43.

Bougara, A., C. Lynsdale, and N.B. Milestone, Reactivity and performance of blastfurnace slags of differing origin. Cement and Concrete Composites, 2010. 32(4): p. 319-324.

Chen, J.J., et al., Solubility and structure of calcium silicate hydrate. Cement and Concrete Research, 2004. 34(9): p. 1499-1519.

Chen, W, and H. J. H. Brouwers. The hydration of slag, part 1: reaction models for alkali-activated slag. Journal of materials science42.2 (2007): 428-443.

Criado, M., et al., Influence of slag composition on the stability of steel in alkali-activated cementitious materials. Journal of Materials Science, 2017. 53(7): p. 5016-5035.

Damidot, D., et al., Thermodynamics and cement science. Cement and Concrete Research, 2011. 41(7): p. 679-695.

De Weerdt, K., et al., Hydration mechanisms of ternary Portland cements containing limestone powder and fly ash. Cement and Concrete Research, 2011. 41(3): p. 279-291.

GB/T 176-2008 Methods for chemical analysis of cement 2008: Beijing. China.

GB175-2007 Common Portland cement. 2007: Beijing. China.

Gong, K. and C.E. White, Impact of chemical variability of ground granulated blast-furnace slag on the phase formation in alkali-activated slag pastes. Cement and Concrete Research, 2016. 89: p. 310-319.

Gruskovnjak, A., et al., Hydration of alkali-activated slag: comparison with ordinary Portland cement. Advances in cement research, 2006. 18(3): p. 119-128.

Jennings, H.M., Aqueous Solubility Relationships for lhvo Types of Calcium Silicate Hydrate. Journal of the American Ceramic Society, 1986. 69(8): p. 614-618.

Jia, S. and I.G. Richardson, Micro- and nano-structural evolutions in white Portland cement/pulverized fuel ash cement pastes due to deionized-water leaching. Cement and Concrete Research, 2017.

Kulik, D.A., et al., GEM-Selektor geochemical modeling package: revised algorithm and GEMS3K numerical kernel for coupled simulation codes. Computational Geosciences, 2012.

Kulik, D.A., Improving the structural consistency of C–S–H solid solution thermodynamic models. Cement and Concrete Research, 2011. 41(5): p. 477-495.

Lee, H.X.D., H.S. Wong, and N.R. Buenfeld, Effect of alkalinity and calcium concentration of pore solution on the swelling and ionic exchange of superabsorbent polymers in cement paste. Cement and Concrete Composites, 2018. 88: p. 150-164.

Lloyd, R.R., J.L. Provis, and J.S.J. van Deventer, Pore solution composition and alkali diffusion in inorganic polymer cement. Cement and Concrete Research, 2010. 40(9): p. 1386-1392.

Lothenbach, B. and F. Winnefeld, Thermodynamic modelling of the hydration of Portland cement. Cement and Concrete Research, 2006. 36(2): p. 209-226.

Lothenbach, B., Le Saout, G., Gallucci, E. and Scrivener, K., Influence of limestone on the hydration of Portland cements. Cement and Concrete Research, 2008. 38(6): p. 848-860.

Lothenbach, B., Matschei, T., Möschner, G. and Glasser, F.P., Thermodynamic modelling of the effect of temperature on the hydration and porosity of Portland cement. Cement and Concrete Research,38(1): p.1-18.

Lothenbach, B., K. Scrivener, and R.D. Hooton, Supplementary cementitious materials. Cement and Concrete Research, 2011. 41(12): p. 1244-1256.

Lothenbach, B., Thermodynamic equilibrium calculations in cementitious systems. Materials and Structures, 2010. 43(10): p. 1413-1433.

Ma, Q., et al., Chloride transport and the resulting corrosion of steel bars in alkali activated slag concretes. Materials and Structures, 2015. 49(9): p. 3663-3677.

Midgley, H.G. and P.B. Rao, Formation of strätlingite, 2CaO.SiO2.Al2O3.8H2O, in relation to the hydration of high alumina cement. Cement and Concrete Research, 1978. 8: p. 169-172.

Myers, R.J., et al., Solution chemistry of cubic and orthorhombic tricalcium aluminate hydration. Cement and Concrete Research, 2017. 100: p. 176-185.

Myers, R.J., et al., Thermodynamic modelling of alkali-activated slag cements. Applied Geochemistry, 2015. 61: p. 233-247.

Oh, S. and Y.C. Choi, Superabsorbent polymers as internal curing agents in alkali activated slag mortars. Construction and Building Materials, 2018. 159: p. 1-8.

Park, J.W., K.Y. Ann, and C.-G. Cho, Resistance of Alkali-Activated Slag Concrete to Chloride-Induced Corrosion. Advances in Materials Science and Engineering, 2015. 2015: p. 1-7.

Provis, J.L., A. Palomo, and C. Shi, Advances in understanding alkali-activated materials. Cement and Concrete Research, 2015. 78: p. 110-125.

Rajabipour, F. and J. Weiss, Electrical conductivity of drying cement paste. Materials and Structures, 2006. 40(10): p. 1143-1160.

Rashad, A.M., et al., Hydration and properties of sodium sulfate activated slag. Cement and Concrete Composites, 2013. 37: p. 20-29.

Richardson, I.G. and J.G. Cabrera, The nature of C–S–H in model slag-cements. Cement and Concrete Composites, 2000. 22: p. 259-266.

Richardson, I.G. and S. Li, Composition and structure of an 18-year-old 5M KOH-activated ground granulated blast-furnace slag paste. Construction and Building Materials, 2018. 168: p. 404-411.

Richardson, I.G., et al., Hydration of water- and alkali-activated white Portland cement pastes and blends with low-calcium pulverized fuel ash. Cement and Concrete Research, 2016. 83: p. 1-18.

Richardson, I.G., Tobermorite/jennite- and tobermorite/calcium hydroxide-based models for the structure of C–S–H: applicability to hardened pastes of tricalcium silicate, β-dicalcium silicate, Portland cement, and blends of Portland cement with blast-furnace

slag, metakaolin, or silica fume. Cement and Concrete Research, 2004. 34(9): p. 1733-1777.

Rothestein, D., et al., Solubility behavior of Ca-, S-, Al-, and Si-bearing solid phases in Portland cement pore solutions as a function of hydration time. Cement and Concrete Research, 2002. 32: p. 1663-1671.

Roy, A., Sulfur speciation in granulated blast furnace slag: An X-ray absorption spectroscopic investigation. Cement and Concrete Research, 2009. 39(8): p. 659-663.

Sangha C.M., et al., Sulphide content variability in cement pastes containing ground granulated blastfurnace slag. Cement and Concrete Research, 1992. 22: p. 181-185.

Scrivener, K.L., P. Juilland, and P.J.M. Monteiro, Advances in understanding hydration of Portland cement. Cement and Concrete Research, 2015. 78: p. 38-56.

Shi, C., A.F. Jiménez, and A. Palomo, New cements for the 21st century: The pursuit of an alternative to Portland cement. Cement and Concrete Research, 2011. 41(7): p. 750-763.

Snydera K.A., et al., Estimating the electrical conductivity of cement paste pore solutions from OH–,K+, and Na+ concentrations. Cement and Concrete Research, 2003. 33: p. 793-798.

Song, S. and H.M. Jennings, Pore solution chemistry of alkali-activated ground granulated blast-furnace slag. cement and Concrete Research, 1999. 29: p. 159-170.

Sun, H., et al., Effects of alkali sulfates in clinker on hydration and hardening performance of Portland cement. Advances in Cement Research, 2018. 30(4): p. 172-184.

Tänzer, R., A. Buchwald, and D. Stephan, Effect of slag chemistry on the hydration of alkali-activated blast-furnace slag. Materials and Structures, 2014. 48(3): p. 629-641.

Taylor, H.F.W., Cement chemistry 2nd edition. 1997, London, UK: Thomas Telford

Thomas, J.J., et al., Effect of hydration temperature on the solubility behavior of Ca-, S-, Al-, and Si-bearing solid phases in Portland cement pastes. Cement and Concrete Research, 2003. 33(12): p. 2037-2047.

Tres Thoenen, et al., The Nagra-PSI Chemical Thermodynamic DataBase 12-07. 2014, Paul Scherrer Institute: Switzerland.

Vicente, M.E.S.d., The Concept of Ionic Strength Eighty Years after Its Introduction in Chemistry. Journal of Chemical Education, 2004. 81(5): p. 750-753.

Vollpracht, A., et al., The pore solution of blended cements: a review. Materials and Structures, 2015. 49(8): p. 3341-3367.

Xu, D., et al., On the future of Chinese cement industry. Cement and Concrete Research, 2015. 78: p. 2-13.

Yang, K., et al., Establishment of a preconditioning regime for air permeability and sorptivity of alkali-activated slag concrete. Cement and Concrete Composites, 2016. 73: p. 19-28.

Ye, H. and A. Radlińska, Shrinkage mitigation strategies in alkali-activated slag. Cement and Concrete Research, 2017. 101: p. 131-143.

Yu, C. H., A Review of CO_2 Capture by Absorption and Adsorption. Aerosol and Air Quality Research, 2012.

Yu, L., et al., Development of chloride-induced corrosion in pre-cracked RC beams under sustained loading: Effect of load-induced cracks, concrete cover, and exposure conditions. Cement and Concrete Research, 2015. 67: p. 246-258.

Zhang, J., et al., The role of sulfide in the immobilization of Cr(VI) in fly ash geopolymers. Cement and Concrete Research, 2008. 38(5): p. 681-688.

Zhang, M., et al., Immobilization potential of Cr(VI) in sodium hydroxide activated slag pastes. J Hazard Mater, 2017. 321: p. 281-289.

Zhu, X.H, et al., Characterisation of pore structure development of alkali-activated slag cement during early hydration using electrical responses. Cement and Concrete Composites, 2018. 89: p. 139-149.

Zhu, X.H, et al., Effect of $Ca(OH)_2$ on shrinkage characteristics and microstructures of alkali-activated slag concrete. Construction and Building Materials, 2018. 175: p. 467-482.

Zhu, X.H., et al., Effect of graphene oxide on the mechanical properties and the formation of layered double hydroxides (LDHs) in alkali-activated slag cement. Construction and Building Materials, 2017. 132: p. 290-295.

Accepted manuscript doi:
10.1680/jadcr.18.00202

Table 1 Thermodynamic fitting parameters for activity coefficient calculation

Ion species	Deby-Hückel å	Deby-Hückel bγ
Ca^{2+}	5	0.165
H^{+}	9	0
K^{+}	4	0.075
Na^{+}	4	0.075
SO_4^{2-}	5	-0.04

Table 2 Thermodynamic data for the solubility calculations (25 °C)

Phases or species	Formation or reaction	log Ksp	ΔH_r(kJ/mol)
OH-	$H_2O - H^{+}$	-14.00	55.81
$CaOH^{+}$	$Ca^{2+} + OH^-$	1.18	21.66
$CaSO_4$	$Ca^{2+} + SO_4^{2-}$	2.11	5.44
$NaSO_4^-$	$Na^{+} + SO_4^{2-}$	0.70	4.69
KSO_4^-	$K^{+} + SO_4^{2-}$	0.85	9.42
$H_3SiO_4^-$	$H_4SiO_4^0 - H^{+}$	-9.83	25.61
$H_4SiO_4^{2-}$	$H_4SiO_4^0 - 2{\cdot}H^{+}$	-23.00	73.64
Portlandite	$Ca^{2+} + 2{\cdot}OH^-$	-5.18	-17.89
Gypsum	$Ca^{2+} + SO_4^{2-} + 2{\cdot}H_2O$	-4.58	-0.46
Ettringite (AFt)	$6{\cdot}Ca^{2+} + 3 + 2{\cdot}Al(OH)_4^- + 4{\cdot}OH^- + 26{\cdot}H_2O$	-45.00	204.5
Monosulphoaluminate (AFm)	$4{\cdot}Ca^{2+} + SO_4^{2-} + 2{\cdot}Al(OH)_4^- + 4{\cdot}OH^- + 6{\cdot}H_2O$	-29.43	45.57
Strätlingite (C2ASH8)	$2{\cdot}Ca^{2+} + 2{\cdot}Al(OH)_4^- + H_4SiO_4^- + OH^- + 2{\cdot}H_2O$	-19.70	-1439.67
Hydrotalcite-OH (MAH10)	$4{\cdot}Mg^{2+} + 2{\cdot}Al(OH)_4^- + 6{\cdot}OH^- + 3{\cdot}H_2O$	-56.02	-103.98
Hydrotalcite-CO_3 (MAcH9)	$4{\cdot}Mg^{2+} + 2{\cdot}Al(OH)_4^- + CO_3^{2-} + 4{\cdot}OH^- + 2{\cdot}H_2O$	-51.14	-351.28
Tobermorite-type CSH	$0.8333{\cdot}Ca^2 + + H_3SiO_4^- + 0.6666OH^- - 0.5{\cdot}H_2O$	-8.0	-1427.56
Jennite-type CSH	$1.6667{\cdot}Ca^{2+} + H_3SiO_4^- + 2.3334{\cdot}OH^- - 0.5667{\cdot}H_2O$	-13.17	-1417.88

Accepted manuscript doi:
10.1680/jadcr.18.00202

Table 3 Chemical compositions of GGBS and PC (%)

Composition	SiO_2	Al_2O_3	Fe_2O_3	MgO	CaO	Na_2O	K_2O	SO_3	Loss
Slag	31.63	13.42	1.32	9.12	36.35	0.34	0.46	0.23	0.61
PC	21.33	5.80	2.57	2.41	60.21	0.21	0.70	2.58	3.27

Table 4 Mix proportions of the pastes tested in this study

Sample type	Binder proportion (wt. %)		Activator concentration (wt. % binder)	Water/binder ratio
	GGBS	PC		
Paste	100	-	5	0.35
	100	-	5	0.50
	-	100	-	0.35
	-	100	-	0.50

Figure captions

Figure 1 Process of pore solution collection

Figure 2 Elements concentrations development as a function of time in both AAS and PC pastes

Figure 3 (a) Ionic strength and (b) total alkalinity development in AAS and PC pastes pore solutions

Figure 4 Effective saturation indices (ESI) of minor or trace hydration products calculated from ions concentration in paste pore solutions

Figure 5 Effective saturation indices (ESI) of major hydration products (J-based and T-based CSH) calculated from ions concentration in pore solutions

Figure 6 Relationship between OH^- concentrations and Ca^{2+} concentrations in the pore solution of AAS and PC pastes

Figure 7 Solubility curves of CSH gels in the aqueous phase

Accepted manuscript doi:
10.1680/jadcr.18.00202

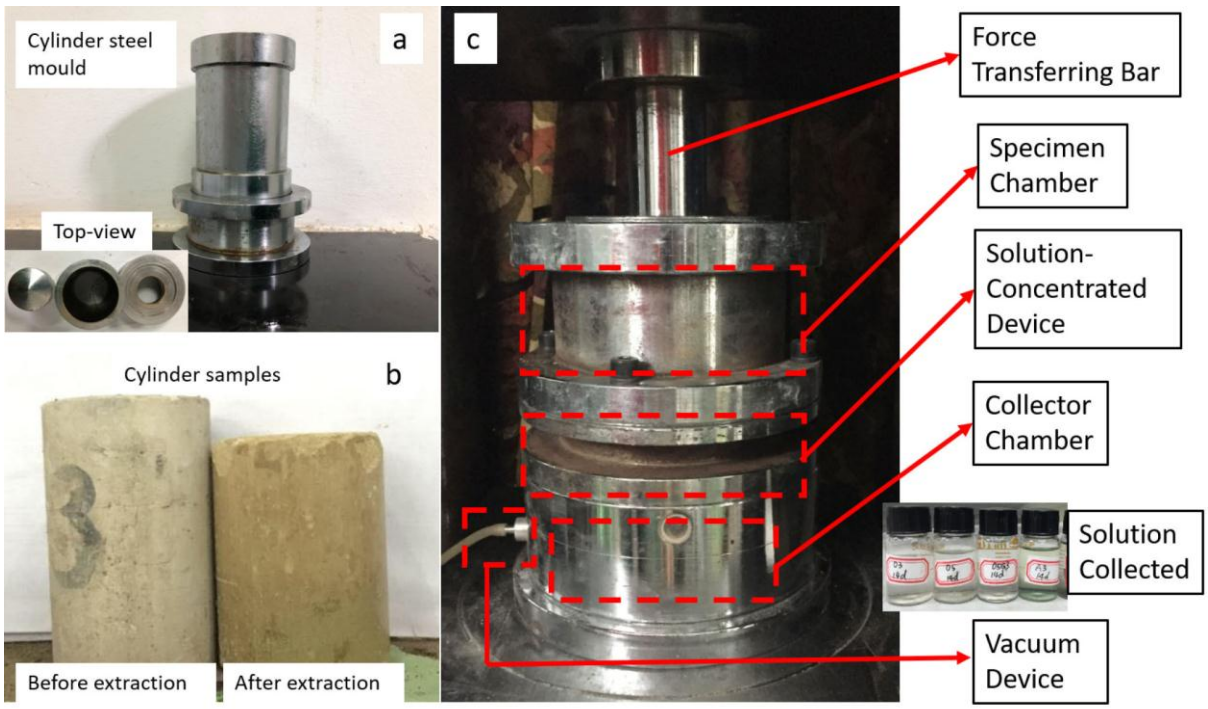

figure 1.tif

Accepted manuscript doi:
10.1680/jadcr.18.00202

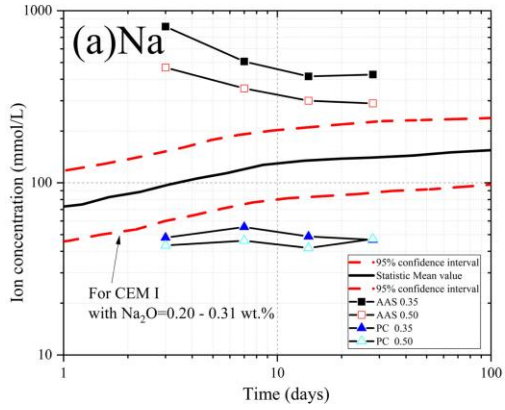

Figure 2-a.Na.tif

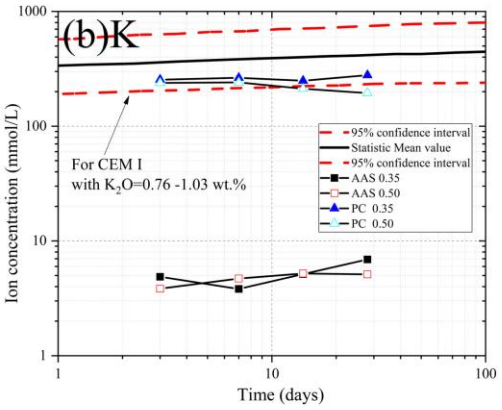

Figure 2-b.K.tif

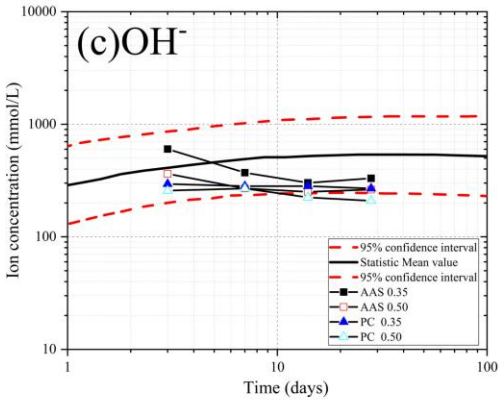

Figure 2-c.OH.tif

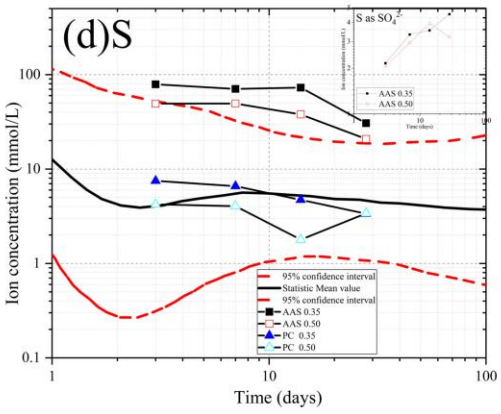

Figure 2-d. S.tif

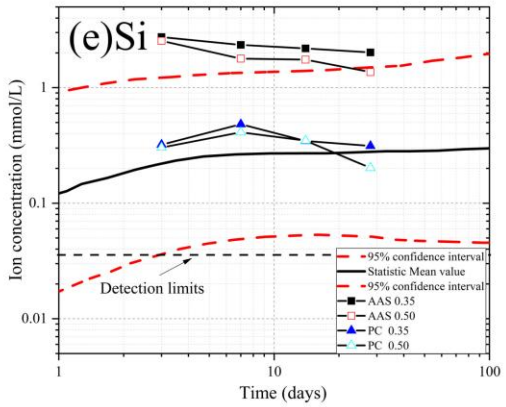

Figure 2-e. Si.tif

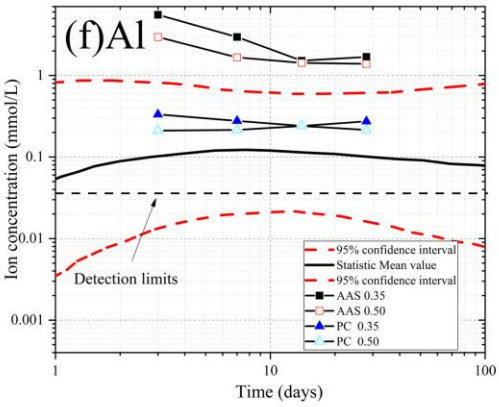

Figure 2-f. Al.tif

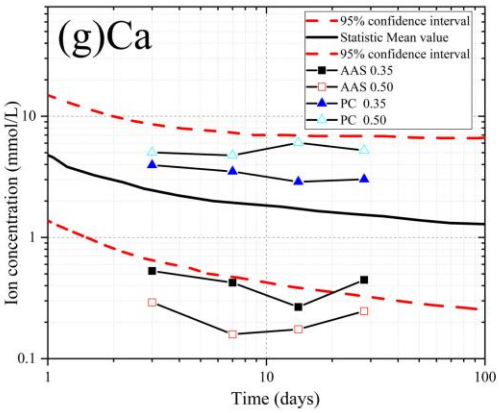

Figure 2-g. Ca.tif

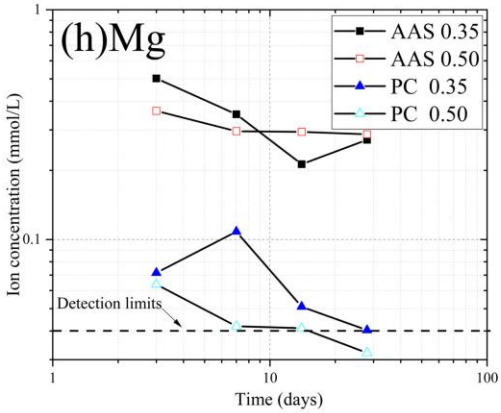

Figure 2-h. Mg.tif

Accepted manuscript doi:
10.1680/jadcr.18.00202

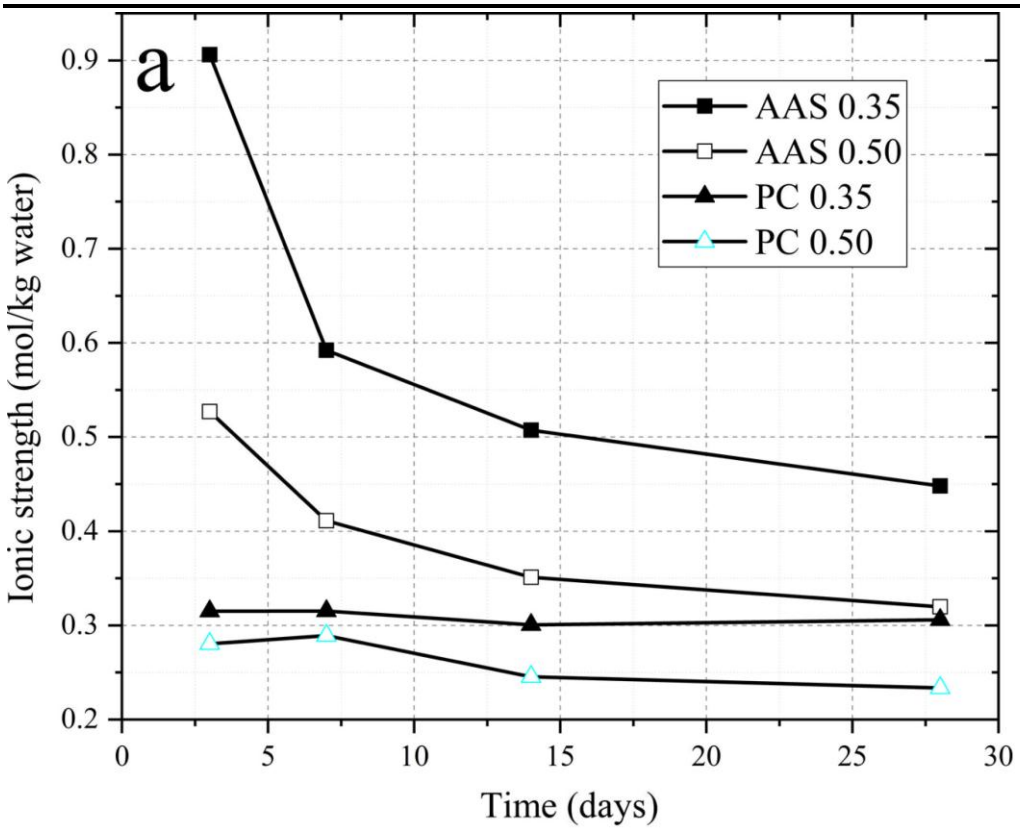

Figure 3-a Ionic strength.tif

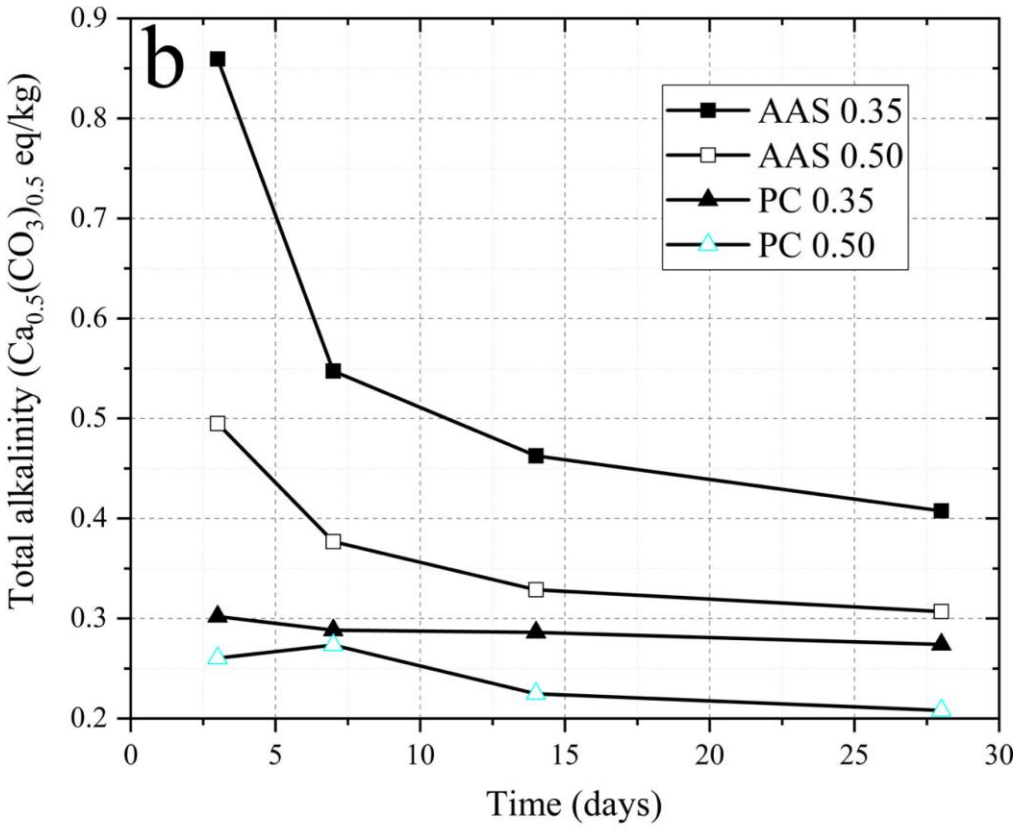

Figure 3-b Alkalinity.tif

Accepted manuscript doi:
10.1680/jadcr.18.00202

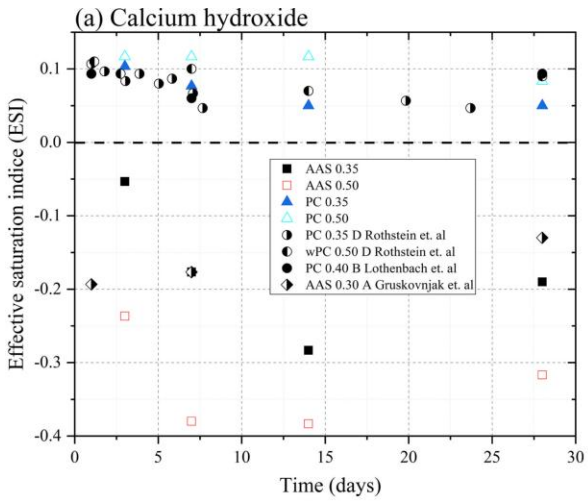

Figure 4-a.ESICH.tif

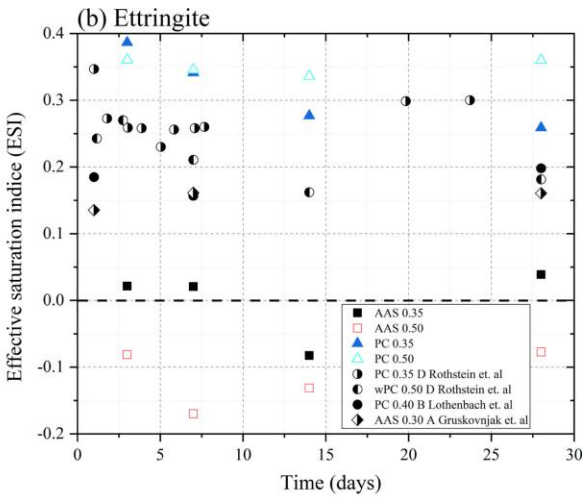

Figure 4-b.ESIaft.tif

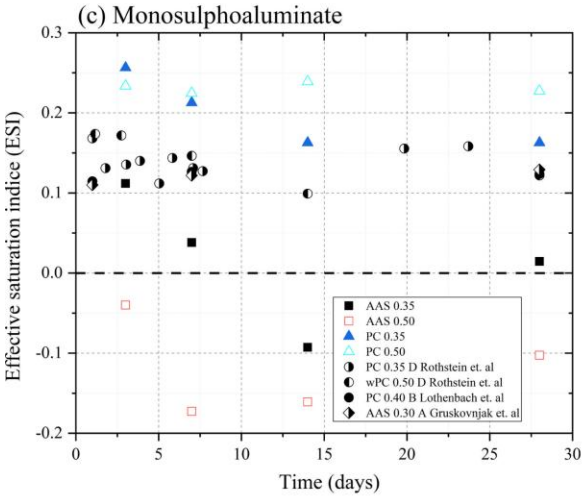

Figure 4-c. ESIafm.tif

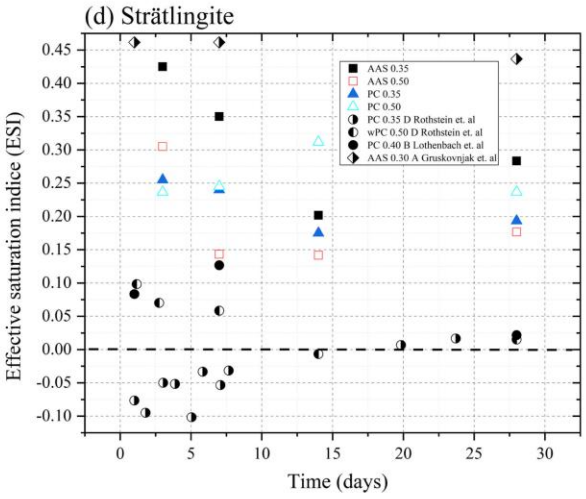

Figure 4-d.ESIstratlingite.tif

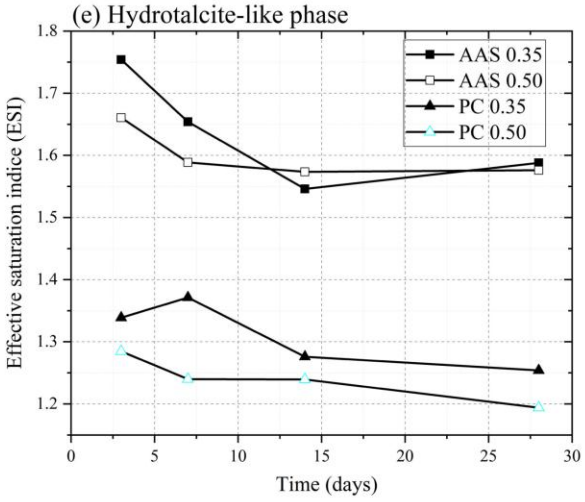

Figure 4-e.ESIHydrotalcite.tif

Accepted manuscript doi:
10.1680/jadcr.18.00202

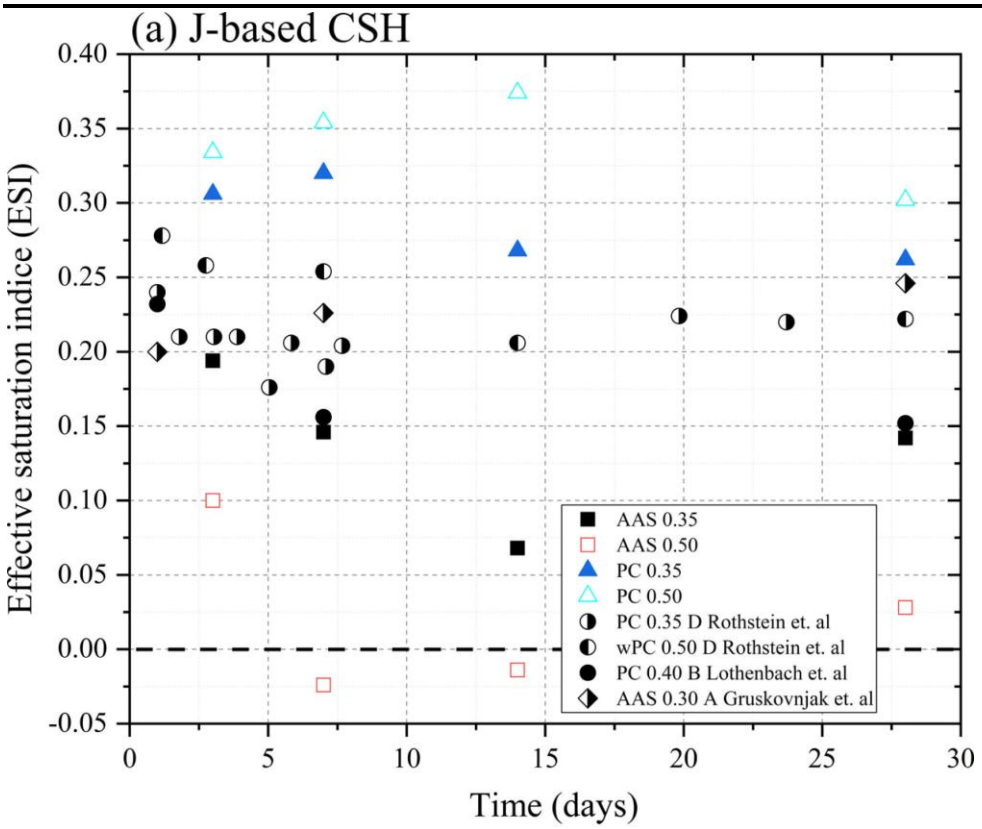

Figure 5-a.ESIJ-based.tif

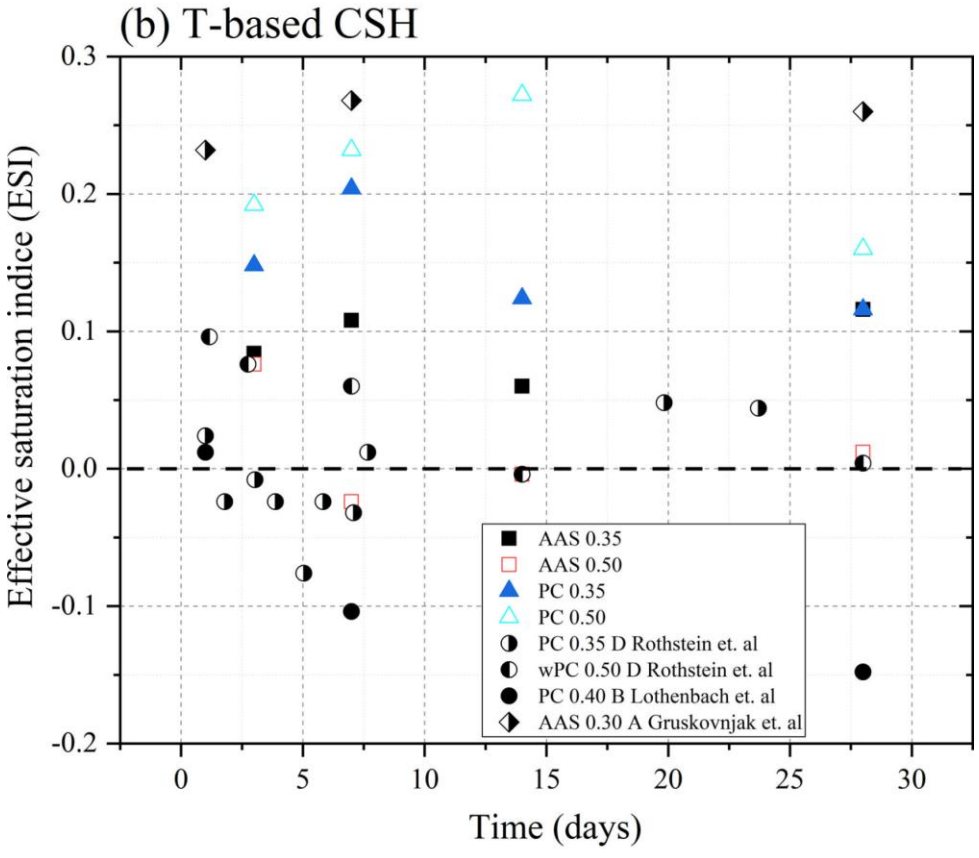

Figure 5-b.ESITbasedcsh.tif

Accepted manuscript doi:
10.1680/jadcr.18.00202

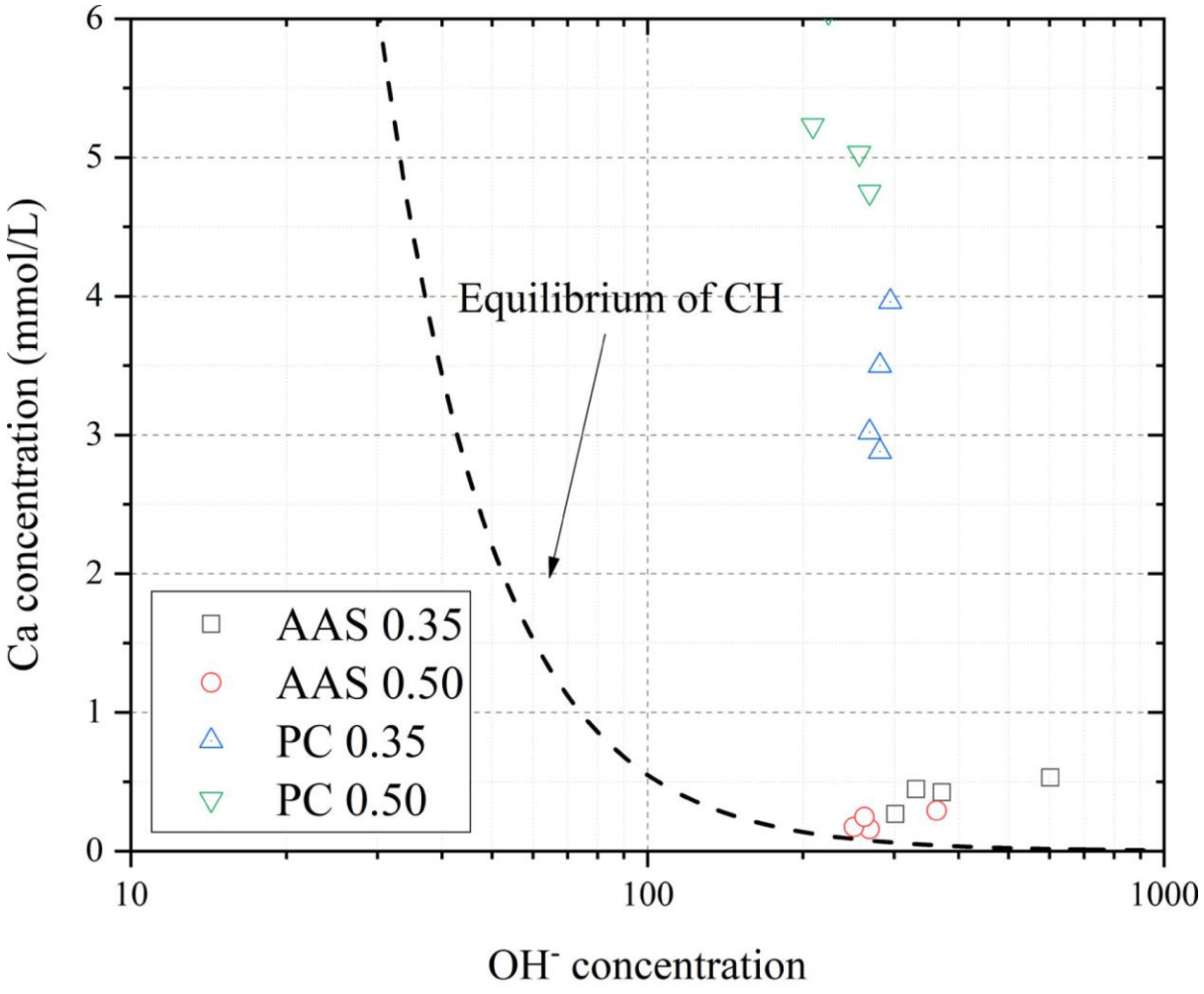

figure 6.tif

Accepted manuscript doi:
10.1680/jadcr.18.00202

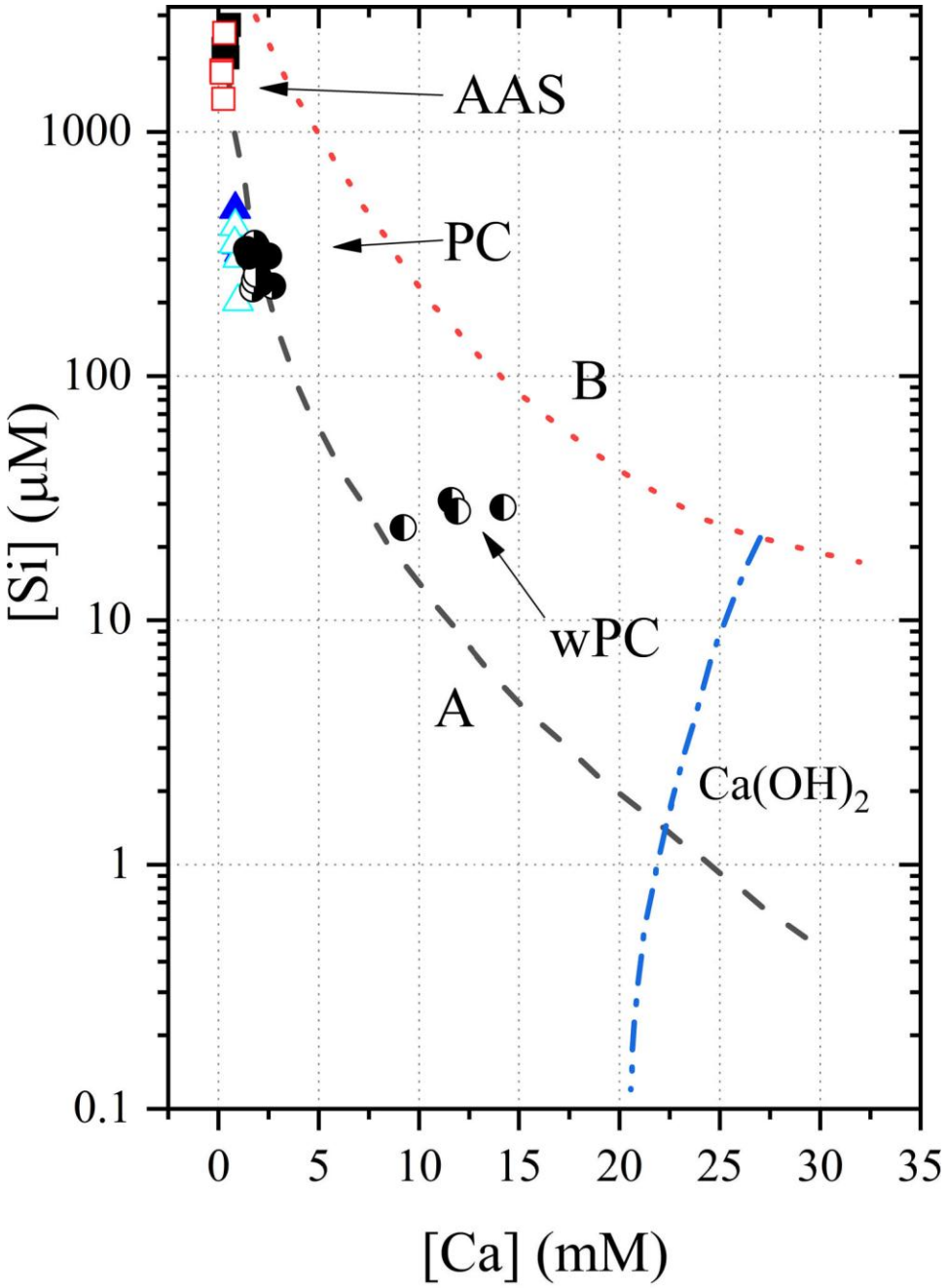

figure 7.tif